Energy Landscape and Isotropic Tensile Strength of *n*-Alkane Glasses

Vincent K. Shen, Pablo G. Debenedetti,* and Frank H. Stillinger†

Department of Chemical Engineering, Princeton University, Princeton, New Jersey 08544

Received: May 21, 2002; In Final Form: August 5, 2002

We report results from a systematic simulational study of the ultimate mechanical strength of *n*-alkane glasses for carbon numbers $n = 1, 2, 3, 4, 6, 8, 16, 24$, and 48. The ultimate isotropic tensile strength was determined by constructing the equation of state of energy landscape for this homologous series. The tensile strength depends nonmonotonically on carbon number, exhibiting a maximum at $n = 3$. The mass density at which fracture occurs initially increases with chain length and then reaches a plateau value for $n > 8$. The predictions of the landscape equation of state are entirely consistent with results generated by a direct inherent structure deformation procedure. Although the ultimate isotropic tensile strength maximum at $n = 3$ would seem to contradict physical intuition regarding chain entanglement, we present a simple mean-field theory that reveals the underlying physics responsible for the tensile strength maximum, namely the simple competition between intermolecular interactions and intramolecular packing effects.

I. Introduction

The vitreous state of matter is ubiquitous in modern technology. For example, waveguides composed of pure, glassy silica provide the infrastructure for high-speed fiber optic networks.[1] In the pharmaceutical industry, glassy matrices composed of sugar and water are used to store and preserve labile proteins.[2] Most polymeric engineering plastics are amorphous solids, and their manufacture serves as a major driving force in the chemical industry. Bulk metallic glasses have been shown to exhibit levels of mechanical strength substantially higher than even the most carefully processed conventional metals and ceramics.[3,4] Combined with their relatively low electrical conductivity, high corrosion resistance, and low density, this particular family of glasses offers exciting possibilities for high-performance materials in the future. Despite its widespread technological utility and promising prospects, the vitreous state remains the most poorly understood state of matter at the molecular level.

Although much theoretical work remains to be done to explain the microscopic mechanisms underlying the extraordinary viscosity slow-down that is the hallmark of the glass transition, a number of practical routes to the glassy state are known, ranging from vapor deposition to ion implantation and cold compression of crystals.[5−7] Historically, the most common route to the glassy state is to supercool a liquid fast enough to avoid crystallization. The resulting material lacks long-range crystalline order, and its properties are closely related to those of its precursor, the supercooled liquid. However, what distinguishes a glass from a liquid is its ability to resist shear deformation. In other words, glasses exhibit proportionality between stress and deformation: they deform reversibly under shear and possess a shear modulus, much like crystalline solids. Unlike crystalline materials, and because they possess inherently liquidlike disorder, glasses tend to exist in bulk form as homogeneous solids devoid of microscopic defects and microstructural heterogeneities that their polycrystalline analogues possess, and which facilitate void nucleation or crack propagation. The important consequence of this is that amorphous solids can exhibit surprisingly high mechanical strength.

Ultimate mechanical strength is an important material property to consider in any engineering application. Experimental determination of a material's ultimate strength is commonly done dynamically, by deforming a specimen at a fixed rate of strain until mechanical failure occurs.[8,9] The ultimate strength is the stress at the point of failure. Because the results are sensitive to the experimental parameters, such as strain rate and specimen size, several measurements are usually performed to obtain reliable statistics. However, destructive testing can be potentially expensive, especially for materials that are difficult to produce, and it is thus desirable to predict their ultimate mechanical properties by nondestructive means. Theory and simulation can play a useful role in this respect. Because most practical theories for glasses, in particular those describing their mechanical properties, remain phenomenological,[10] computer simulation presents itself as a useful alternative not only for predicting the properties of these materials, but also for aiding in the development of rigorous, microscopic theory.

In this spirit, there has been considerable effort devoted toward predicting the ultimate tensile strength of engineering materials. Because their atomic positions can be determined experimentally, crystalline solids have historically been the focus of such studies. Traditionally, the study of material strength in a lattice has been formulated as a stability problem.[11] More recently, at the microscopic-length scale, significant effort has been devoted toward predicting the tensile and shear strength of crystalline solids using sophisticated *ab initio* and quantum mechanical simulations.[12−17] Although much of this work, in addition to classical simulation studies, has provided important insight into failure mechanisms operating in ideal solids,[18−26] there still remains significant disagreement between computational predictions and experimental measurement.[13]

Because glasses possess history-dependent structure and are hence not in equilibrium, they pose difficulties for theoretical and computational modeling not encountered with crystals. Polymeric systems have received special attention due to their

* To whom correspondence should be addressed. E-mail: pdebene@princeton.edu.

† Department of Chemistry, Princeton University.

10.1021/jp021247g CCC: $22.00
Published on Web 09/13/2002

industrial prominence.[27−29] *Ab initio* molecular dynamics studies have focused on the rupture strength of the carbon−carbon bond in simple *n*-alkane chains in various conformations but are limited to systems of only a few molecules.[30−33] Kinetic Monte Carlo methods,[34,35] which are capable of incorporating a variety of failure mechanisms, such as bond rupture and chain slippage, have proven quite useful in modeling the actual experimental tensile strength protocol, but at the outset assume rate laws for the microscopic mechanisms included in the simulation. In such an approach, because the microscopic structure is unknown, a very coarse-grained representation of the amorphous network is employed.[36−38]

Since its introduction, the energy landscape formalism[39,40] has provided valuable insight into the molecular-level phenomena occurring in supercooled liquids and glasses.[41,42] However, only in recent years has the connection between the landscape and the mechanical properties of glasses been demonstrated.[43−45] In particular, it is the so-called equation of state of the energy landscape that bridges the gap between the two, and it is this *thermodynamic* construction that can be exploited to predict the ultimate strength of glassy materials. Thus far, investigations of the ultimate isotropic tensile strength of glasses have been limited to monatomic fluids,[43,46] water,[47] and simple hydrocarbons.[48] What remains unknown is the connection between molecular architecture and mechanical strength. Elucidation of this relationship requires systematic study, and as a starting point, we have performed such a study for the *n*-alkane glasses. Interest here in the *n*-alkanes is motivated by the fact that these simple linear hydrocarbons exhibit a rich range of thermodynamic behavior as a function of the simplest molecular parameter, namely chain length *n*. For example, surface-freezing phenomena[49−53] and the even−odd effect[54] in their freezing temperatures have recently received special attention. Their critical pressure and mass density exhibit maxima at $n = 2$ and 6,[55−57] respectively, and display power-law dependence for large *n*.[58] Furthermore, the *n*-alkanes serve as a convenient starting point for studying amorphous polymeric systems.

In this paper, we present results from a systematic study of the ultimate isotropic tensile strength of the *n*-alkane glasses using the energy landscape formalism. The most striking result of this work is that the strength within this family of glasses is maximized at $n = 3$. The outline of this paper is as follows. Section II reviews the landscape formalism and its relation to the mechanical strength of glasses. Section III describes the simulation model for the *n*-alkanes and methods used in this study. Results and discussion are presented in Section IV. Finally, Section V contains the main conclusions and lists the open questions suggested by this work.

II. Energy Landscape/Inherent Structure Formalism

The potential energy hypersurface or energy landscape, $\Phi(\boldsymbol{r}^N)$, is simply the relationship between a system's total potential energy and its degrees of freedom, and it naturally contains all the physics that govern its dynamics and thermodynamics. Although the complexity of this surface precludes its detailed description in all but the simplest systems, significant simplification can be achieved by configurational mapping to topologically important features in the landscape, namely potential energy minima. By definition, these minima are mechanically stable, and provided that every point in configuration space (with the possible exception of a zero-measure subset) can be mapped uniquely to a minimum, they represent the mechanically stable atomic packings that a system inherently samples as it explores configuration space. Accordingly, these local potential energy minima are called inherent structures, and configurations that map to the same minimum are collectively referred to as a basin of attraction. Given a unique configurational mapping process, it can be rigorously shown that the thermodynamics of glasses and supercooled liquids can be described in terms of the distribution of inherent structure energies;[39] at the same time, dynamics are related to transitions between basins.[59] Within the energetic hierarchy of this formalism, it naturally follows that crystalline solids are systems occupying the lowest-lying energy basins; glasses are systems trapped within amorphous inherent structures whose energies are higher than that of the crystal; and deeply supercooled liquids are systems that move infrequently between amorphous basins.

Mathematically, for a system of *N* atoms in the canonical ensemble, the simplest configurational mapping takes each atom *i* along a steepest descent path[39,40]

$$\frac{d\boldsymbol{r}_i}{ds} = -\frac{\partial\Phi}{\partial\boldsymbol{r}_i} \qquad (1 \le i \le N) \tag{1}$$

where $\boldsymbol{r}_i$ is the coordinate vector of atom *i*, Φ is the total potential energy of the system, and *s* is a generic progress variable. As $s \rightarrow \infty$, solutions to these equations satisfy mechanical equilibrium

$$\frac{\partial\Phi}{\partial\boldsymbol{r}_i} = 0 \qquad (1 \le i \le N) \tag{2}$$

It should be emphasized that because the potential energy is an explicit function of atomic coordinates, it is therefore an implicit function of bulk density.[60] Notice that this configurational mapping procedure corresponds to the physical process of making a glass by cooling or quenching a fluid instantaneously to $T = 0$. Thus, the properties of a system's inherent structures are intimately related to those of its glass.

The connection between the landscape and macroscopic properties of a glass is provided by the equation of state of the energy landscape, that is to say average inherent-structure pressure P_{IS} as a function of bulk density.[44] It is precisely this thermodynamic construction that is exploited here as a method to determine the ultimate isotropic tensile strength of a glass. Because a glass is a liquid trapped within a potential energy minimum or inherent structure, the equation of state of the energy landscape physically corresponds to the equation of state of a liquid in the $T = 0$ limit. In the canonical ensemble, construction of the landscape equation of state involves taking configurations from a thermally equilibrated simulation at some temperature and density, minimizing their potential energies by eq 1, and then calculating the average inherent-structure pressure. This procedure is repeated at other densities, while maintaining the same equilibration temperature. Although the equilibration temperature affects the average inherent-structure energy, that is the average basin depth the system samples, the equation of state of the landscape (pressure vs density) is largely insensitive to it as long as the equilibration temperature is sufficiently high (i.e., greater than the critical temperature). A notable exception is water whose energy landscape is usually studied under conditions where the liquid is supercooled and therefore exhibits slow inter-basin dynamics.[47,61,62] For illustrative purposes, the complete equation of state of the energy landscape for *n*-hexane is shown in Figure 1. It is clear that the landscape equation of state depends nontrivially on density and its shape resembles the isotherms of analytical equations of state for liquids. However, there are two important distinctions. First, although points along an isotherm in a real equation of state

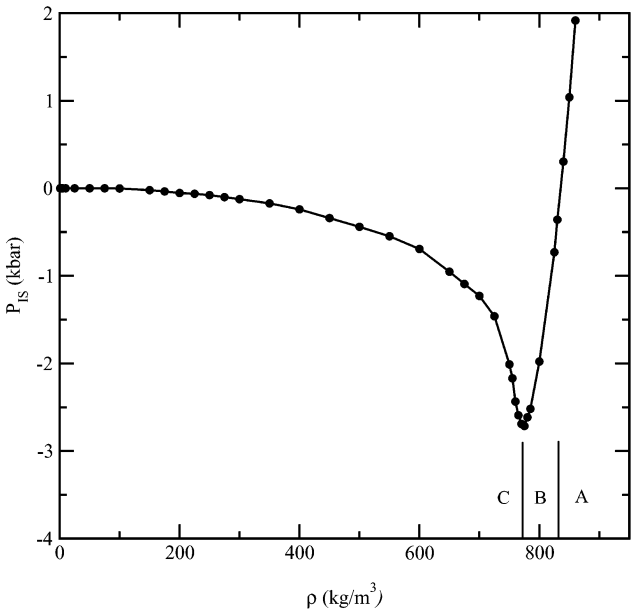

Figure 1. Equation of state of the energy landscape for *n*-hexane. This zero-temperature isotherm can generally be divided into three density regions *A*, *B*, and *C*. In region *A*, $P_{IS} > 0$. In region *B*, $P_{IS} < 0$. In region *C*, the inherent structures are fissured and the packings are spatially inhomogeneous.

are directly connected by a continuum of thermally equilibrated states, points along the equation of state of the landscape are only indirectly connected to each other via the thermally equilibrated simulation runs from which they were obtained. Second, points along the "unstable" portion of the landscape EOS are mechanically stable (i.e., they represent local-minimum energy configurations), whereas corresponding points in analytical equations of state are unphysical (i.e., experimentally unattainable). These subtleties aside, the equation of state of the landscape exhibits behavior that is characteristic of a real equation of state. For example, the density at which the average inherent-structure energy E_{IS} reaches a minimum coincides with the density at which the average inherent-structure pressure P_{IS} is zero.[48] It should be emphasized that although the phrase "equation of state of an energy landscape" has other meanings in the literature,[45] our usage of the phrase in this paper follows the original definition,[44] namely the average inherent structure pressure as a function of bulk density. Physically, this construction can be interpreted as the $T = 0$ isotherm of a liquid, in the sense that the system is equilibrated under conditions where it can sample all energy minima, but its properties are studied upon removal of the kinetic energy.

For systems studied to date,[43,46−48] the equation of state of the landscape can generally be subdivided into three density regions, as shown in Figure 1. The high-density region *A* is characterized by compressed inherent structures. At intermediate densities, region *B*, inherent structures are under isotropic tension. The pressure here decreases with decreasing density until a minimum in pressure is reached. As in region *B*, inherent structures in region *C* are also under tension, but the pressure here increases with decreasing density and eventually vanishes as density approaches zero. The density at which the minimum pressure, ρ_S, is attained is called the Sastry density, ρ_S, and separates region *B* from *C*.

Both P_S and ρ_S are characteristic material properties and have special physical significance. Statistical geometric analyses of inherent structures in atomic and simple molecular fluids have shown that they are spatially heterogeneous below ρ_S, that is to say inherent structures below this limiting density consist of densely packed regions of molecules coexisting with voids or cracks.[43,48] Thus, the Sastry density represents the lowest density at which a homogeneous glass can exist and hence corresponds to the maximally stretched glass. Therefore, the isotropic tension at this density, $-P_S$, is the maximum tension that a homogeneous glass can sustain prior to fracture, otherwise known as its ultimate isotropic tensile strength. These arguments strongly suggest that the Sastry point is the $T = 0$ limit of the superheated liquid spinodal,[43,44] and represents a fundamental limit to homogeneous glass formation. For monatomic fluids equilibrated above their critical temperature, the Sastry point bears a simple yet intriguing relationship to the critical point. The ratio of the Sastry density to critical density is roughly 3, whereas the ratio of the ultimate isotropic tensile strength to critical pressure is approximately -27.[42] An important aspect of this work is to investigate whether such simple relationships hold for molecular fluids.

The equation of state of the energy landscape is not only the means by which to study the mechanical properties of glasses within the landscape formalism. Alternatively, one can probe their mechanical behavior by directly deforming the inherent structures themselves.[27−29,63] By using a series of steps consisting of incremental deformations and subsequent energy minimizations under constant strain, the mechanical response of glasses under various loading conditions can be investigated in the low-temperature limit. Although the majority of these studies have focused on how the underlying landscape changes as a result of structural rearrangements that accompany macroscopic strain, in particular, the relationship between mechanical yielding and the disappearance of energy minima,[60,64,65] such an approach can, in principle, also be used to determine the ultimate mechanical strength of glasses.[66]

We have studied the ultimate isotropic strength of the *n*-alkane glasses using two methods. In the first, the ultimate isotropic strength is determined by constructing the equation of state of the energy landscape and locating the Sastry point. In the second method, high-density inherent structures are processed by a sequence of incremental isotropic expansions and energy minimization steps. This series of steps is repeated until the system fractures, that is to say a minimum in pressure as a function of density is reached. *A priori*, it is unclear how the fracture properties determined by the two processes relate to each other, and hence an important part of this investigation is to clarify this relationship.

III. Simulation Model and Methods

In this work, the *n*-alkanes are modeled as fully flexible chains of united atoms with each interaction site corresponding to a CH_4 molecule or either a $-CH_3$ or $-CH_2-$ group. For a linear chain of united atoms of length *n*, its conformation is completely specified by the set of *n*-1 bond lengths *d*, *n*-2 bond angles θ, *n*-3 dihedral angles ϕ, and three Euler angles (ϑ, Θ, and Ψ) describing the relative orientation of the first two bonds in the chain. This set constitutes the chain's generalized coordinates. In conjunction with the position of the first united atom within the chain, the spatial coordinates of each interaction site can be specified completely by 3*n* degrees of freedom.

Bond stretching and bending are described by harmonic potentials[67,68]

$$u_{\text{stretch}}(d) = K_r(d - d_{\text{eq}})^2/2 \tag{3}$$

$$u_{\text{bend}}(\theta) = K_\theta(\theta - \theta_{\text{eq}})^2/2 \tag{4}$$

TABLE 1: Parameters for the Buckingham Exponential-6 Potential in Lennard−Jones Form

group, i	σ_i [Å]	ϵ_i/k_B [K]	α_i
CH_4	3.741	160.3	15
CH_3	3.679	129.6	16
CH_2	4.000	73.5	22

where $K_r = 96\,500$ K/Å^2, $K_\theta = 62\,500$ K/rad^2, d_{eq} is a species-dependent equilibrium bond length, and θ_{eq} is the equilibrium bond angle which is fixed at 114°.[68] Equilibrium bond lengths for CH_3-CH_3, CH_3-CH_2, and CH_2-CH_2 bonds are set to 1.839, 1.687, and 1.535 Å, respectively.[69] The dihedral angles are governed by a potential of the form[70]

$$u_{tor}(\phi) = V_0 + \frac{V_1}{2}(1+\cos\phi) + \frac{V_2}{2}(1-\cos 2\phi) + \frac{V_3}{2}(1+\cos 3\phi) \tag{5}$$

where $V_0 = 0$, $V_1 = 355.03$ K, $V_2 = -68.19$ K, and $V_3 = 791.32$ K. Within a chain, united atoms separated by more than three bonds interact via the same nonbonded potential that governs the interaction between united atoms on different molecules. In this work, the nonbonded potential is described by the Buckingham exponential-6 potential

$$u_{nb}(r) = \begin{cases} \dfrac{\epsilon}{1-(6/\alpha)}\left[\dfrac{6}{\alpha}\exp\left(\alpha\left[1-\dfrac{r}{r_{min}}\right]\right) - \left(\dfrac{r_{min}}{r}\right)^6\right] & r > r_{max} \\ \infty & r < r_{max} \end{cases} \tag{6}$$

where ϵ is the depth of the potential well, α controls the width of the potential well, r_{min} is the distance at which the potential reaches its minimum, and r_{max} is the smallest distance for which $du_{nb}(r)/dr = 0$, the position of a maximum of the form shown in eq 6. A characteristic diameter σ analogous to that of the Lennard−Jones interaction potential corresponds to the distance at which $u_{nb}(r) = 0$. The advantage of the Buckingham exponential-6 form is that it offers an additional degree of freedom in optimizing the model relative to the traditional Lennard−Jones potential. The parameters for each united atom type are summarized in Table 1. Interaction parameters between different united atom types are obtained by standard arithmetic and geometric averages

$$\sigma_{ij} = \frac{1}{2}(\sigma_i + \sigma_j) \tag{7}$$

$$\epsilon_{ij} = \sqrt{\epsilon_i \epsilon_j} \tag{8}$$

$$\alpha_{ij} = \sqrt{\alpha_i \alpha_j} \tag{9}$$

The total potential energy of the system, Φ, is simply a summation over all of the above energetic contributions.

The above model for the *n*-alkanes was developed and optimized by Errington and Panagiotopoulos[69,71] to fit experimental liquid−vapor equilibrium data. There are two key features to the model. First, the methyl and methylene groups differ in size and possess different energy well depths. In Table 1, it seems counterintuitive that a methyl group should be smaller than a methylene group, but this is actually consistent with other force fields designed for simulating *n*-alkanes.[67,72] Second, adjacent united atoms within the same chain overlap by virtue of specification of the equilibrium bond lengths. It has been shown that these are essential requirements in order for a united atom model to reproduce the maxima in critical pressure and density as a function of chain length.[58] The Buckingham exponential-6 potential was cut and shifted so that the force vanishes smoothly at 15 Å. This was necessary because the energy minimization procedure requires a continuous force for numerical stability. Although this modification changes the potential slightly from its original form, it is expected that deviations from the experimental properties for which the parameters were optimized will be systematic (in the same direction) for all carbon numbers.

To construct the equation of state of the energy landscape for the *n*-alkanes, either configurational-biased Monte Carlo (CBMC)[73,74] or multiple time-step molecular dynamics (MTS MD)[75] simulation was used to generate thermally equilibrated configurations in the canonical ensemble for energy minimization. These more sophisticated simulation methods were required to deal efficiently with the stiff degrees of freedoms in the chains. The choice of simulation was based on computational convenience. A system consisting of 1600−2000 united atoms in a cubic simulation box with periodic boundary conditions was used in all cases. All species were equilibrated at approximately 1.5× the experimental critical temperature, to ensure that the system could in principle sample the overwhelming majority of local energy minima in the landscape. The Monte Carlo simulations consisted of an equilibration period of two million trials followed by a production period in which configurations were saved every 200 000 trials. In the molecular dynamics simulations, the equilibration period lasted for 200 ps using a large and small time step of 2.0 and 0.5 fs, respectively. Temperature was thermostated using a Nose−Hoover chain of length five, and the equations of motion were integrated using an explicit reversible multiple time step integrator as developed by Martyna et al.[76] Configurations were saved every 10 ps for energy minimization. For each species, thirty configurations per state point were generated, with the exception of $n = 48$, where forty configurations were saved to obtain better statistical sampling. Energy minimization was performed using the conjugate gradient method[77] and was terminated when the relative fractional energy difference between the previous and current step was less than 1×10^{-8}.

Investigation of ultimate tensile strength via direct inherent structure deformation was only performed for *n*-alkanes of length $n < 48$. High-density inherent structures corresponding to $P_{IS} = 0$ were taken as the starting configurations. Each of these was expanded isotropically stepwise by 5 kg/m^3 and then its potential energy was minimized. This process was repeated until a minimum in pressure as a function of density was reached. For each chain length, results were averaged over fifteen such runs.

IV. Results and Discussion

We have studied the ultimate isotropic tensile strength of the *n*-alkane glasses by constructing their landscape equations of state. Before proceeding, we first demonstrate that the Sastry point also corresponds to a condition of fracture for complex molecular fluids, such as those investigated here, and not just for atomic systems.[43] Representative inhomogeneous and homogeneous inherent structures for $n = 8$ from both sides of the Sastry density are shown in Figures 2 and 3, respectively. It is clear that the fractured inherent structure, Figure 2, contains significant cavity space, which not surprisingly resembles a crack in the system, whereas the homogeneous inherent structure, Figure 3, is devoid of such defects. The connection between the Sastry point and mechanical strength can be demonstrated quantitatively by statistical geometric analysis of

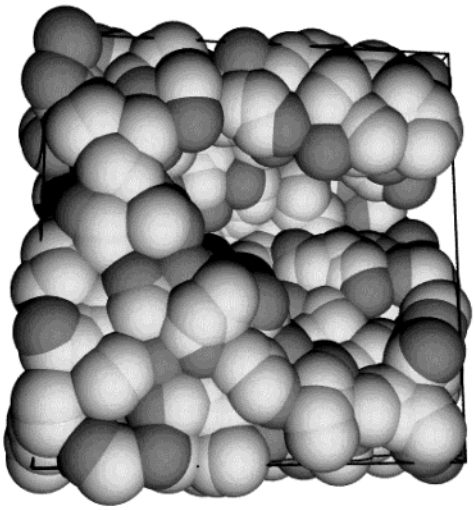

Figure 2. Representative fractured inherent structure for *n*-octane ($\rho < \rho_S$). Dark spheres correspond to methyl groups, and the lighter ones are methylene groups.

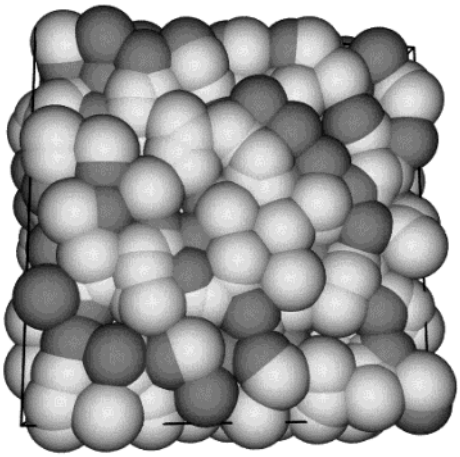

Figure 3. Representative homogeneous inherent structure for *n*-octane ($\rho > \rho_S$). Dark spheres correspond to methyl groups, and the lighter ones are methylene groups.

the void space[78] present in the inherent structures as a function of density. In Figure 4, the average inherent-structure pressure and void fraction are plotted as a function of density for $n = 8$. As in the case for simple fluids, high density inherent structures are spatially homogeneous above ρ_S and inhomogeneous below. More importantly, as the system is expanded isotropically, Figure 4 clearly shows that the density at which cavities begin to form is practically coincident with the density at which the minimum in pressure occurs, namely the Sastry density. Notice that the size of these initial cavities is of the order of atomic dimensions. Because harmonic bonding potentials are used here, bond rupture is precluded as a viable fracture mechanism, and therefore, fracture in this case is driven solely by the relative displacements of individual molecules. The loss of cohesion below ρ_S is directly related to the creation of void space. The physical picture that emerges from these observations is that the Sastry point corresponds to the maximally stretched molecular glass, whereas the pressure at this point is its ultimate isotropic tensile strength, or the maximum tension that can be sustained just prior to fracture. Although results have only been presented for $n = 8$, identical behavior is observed for all chain lengths investigated in this work.

The equations of state of the energy landscape for the *n*-alkanes of chain length $n = 1$, 2, 3, 4, 6, 8, 16, 24, and 48

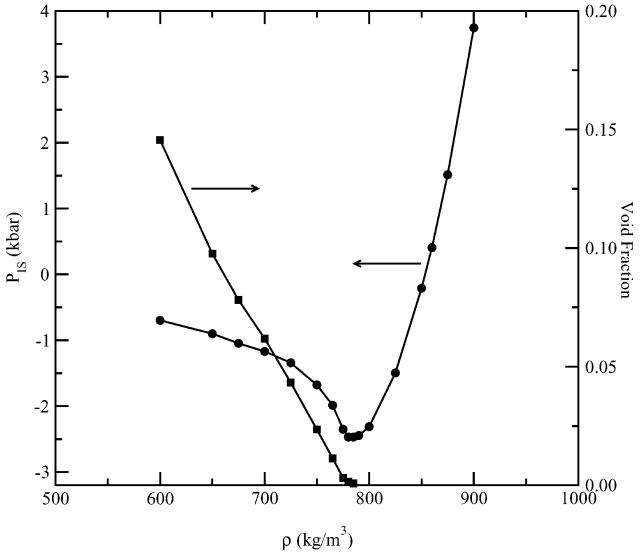

Figure 4. Equation of state of the energy landscape (circles) and the average void volume fraction (squares) in the inherent structures as a function density for *n*-octane, $n = 8$.

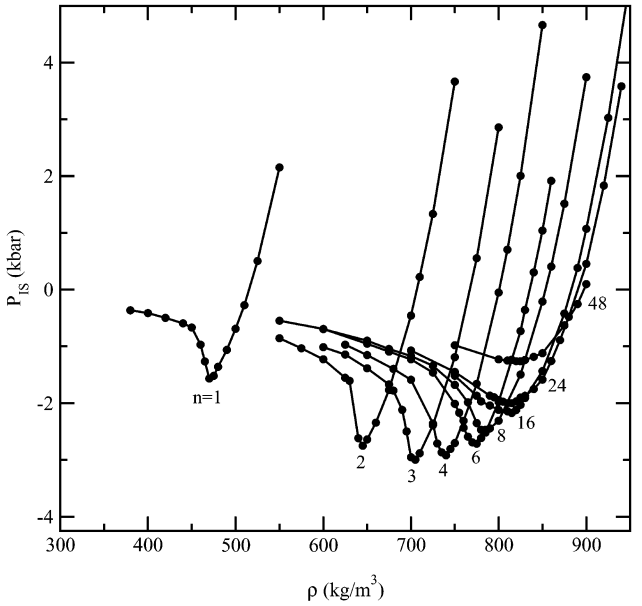

Figure 5. Equations of state of the energy landscape for the *n*-alkanes studied in this work, $n = 1$, 2, 3, 4, 6, 8, 16, 24, and 48.

are shown in Figure 5. All of the curves have similar shapes and extend significantly into the negative pressure region where the system is under isotropic tension. More importantly, notice that pressure on the *y*-axis is given in units of kbar, which is the same order of magnitude as the tensile strength of steel alloys.[8] There are two important trends to glean from Figure 5, namely the chain length dependences of ρ_S and $-P_S$. For clarity, these two quantities are plotted separately as a function of inverse chain length in Figures 6 and 7.

Figure 6 shows that the Sastry density initially increases with chain length but then reaches a plateau value at approximately $n = 16$. This nontrivial chain length dependence is due to the fact that adjacent united atoms within the same chain are actually interpenetrating spheres by virtue of the bonding constraints in the simulation model. Consequently, the volume occupied by *m* unbonded united atoms is larger than that of *m* bonded ones. Because the Sastry density is the lowest density at which a mechanically stable amorphous solid can exist absent of any

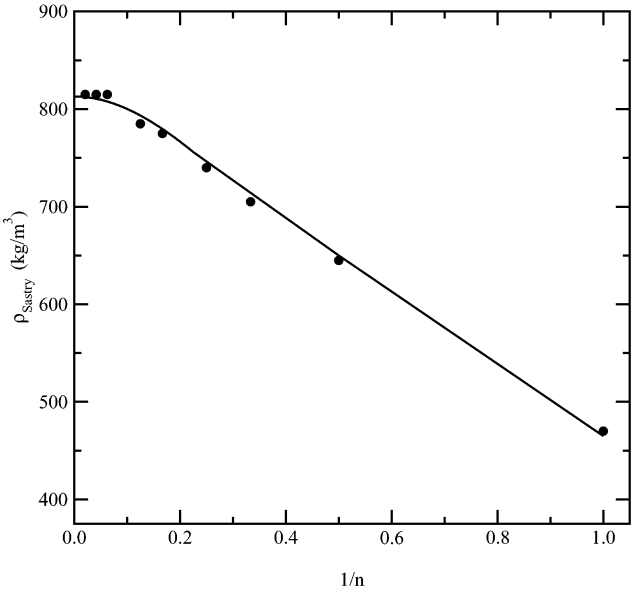

Figure 6. Relationship between the Sastry density and inverse chain length for the *n*-alkanes studied in this work. The line is a guide to the eye.

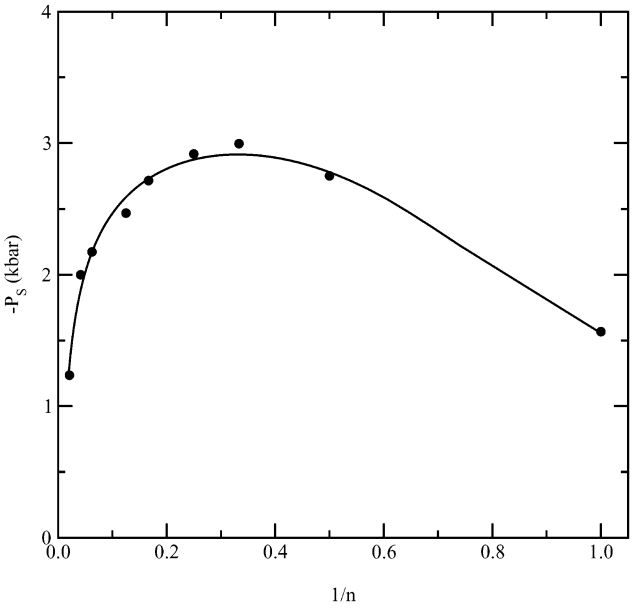

Figure 7. Relationship between the ultimate isotropic tensile strength determined by the landscape equation of state and inverse chain length for the *n*-alkanes studied in this work. The line is a guide to the eye.

void space, this limiting density should at least initially increase with carbon number. Beyond some intermediate chain length, the homogeneous amorphous packing problem that is associated with the Sastry density becomes insensitive to carbon number. In other words, in the long chain limit where n is large, a system composed of chains of length n is indistinguishable from a system composed of chains of length $n+1$ at least from a molecular packing point of view. This naturally gives rise to an asymptotic approach to a limiting value of ρ_S in the limit of large n.

In Figure 7, the ultimate isotropic tensile strength, $-P_S$, is plotted as a function of inverse chain length. There are two striking features to this plot. The first is the tensile strength maximum at $n = 3$, which is reminiscent of the maximum in critical pressure for the *n*-alkanes at $n = 2$. The second is that the isotropic tensile strength decreases with increasing carbon

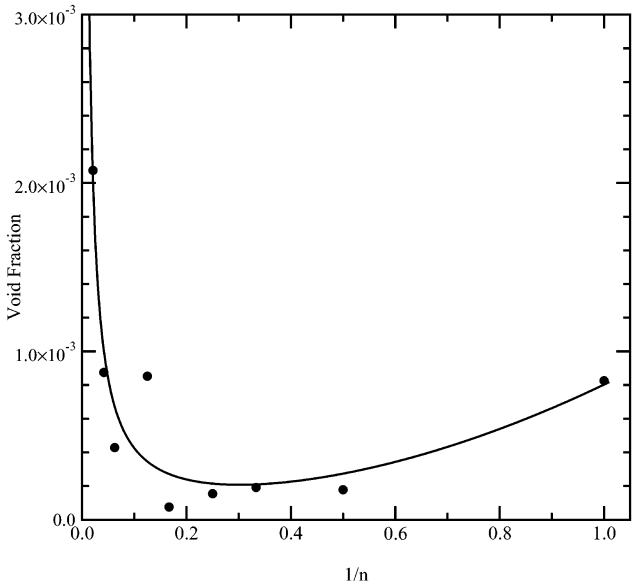

Figure 8. Average void fraction in the *n*-alkane inherent structures at their respective Sastry densities plotted as a function inverse carbon number. The line is a guide to the eye.

number beyond $n = 3$. In contrast, we note that the average inherent structure energy per molecule at the Sastry point ($E_{IS}(\rho_S) < 0$) decreases monotonically with carbon number throughout the entire range of chain lengths studied. The tensile strength results are quite remarkable because physical intuition would lead one to believe that it should in fact increase with carbon number simply due to chain entanglements. Although the degree of chain entanglement is unknown in these systems, work by Saitta and Klein[32] suggests that systems composed of united atom *n*-alkanes are capable of exhibiting some degree of topological chain entanglement starting at $n = 9$ even though they do not display rheological entanglement dynamics. It has been found experimentally that the ultimate tensile strength for amorphous low density, linear polyethylene under uniaxial tension decreases with molecular weight.[79] In reference to previous work on the ultimate isotropic tensile strength of simple hydrocarbons,[48] the complex chain length dependence found here is consistent with the observation that chains of length $n = 2$ and 5 possess very similar tensile strength.

That the ultimate isotropic tensile strength should be maximized at $n = 3$ is not obvious. Because fracture is initiated by voids,[8,9] a statistical geometric analysis of the *n*-alkane glasses at their Sastry density was performed to see if the defects that drive mechanical failure could provide physical insight into the origin of the tensile strength maximum. Details of the geometric algorithm, which allows calculation of the volume, surface area, and connectivity of voids, have been given elsewhere.[78] The average void fraction and defect density are plotted as a function of inverse chain length in Figures 8 and 9, respectively. It is interesting to see that the void fraction at the Sastry density, Figure 8, behaves non-monotonically with chain length. Although this quantity does not correlate perfectly with tensile strength, it too displays an extremum at small chain length. However, the defect density, which is defined as the number of cavities per unit volume at the Sastry point, correlates quite well with tensile strength, exhibiting a minimum near $n = 3$. The observation that the void fraction and defect density at the Sastry point correlate with tensile strength suggests that molecular packing effects play a basic role in determining the relative ultimate mechanical strength of *n*-alkane glasses. This should not be entirely surprising because the manner in which

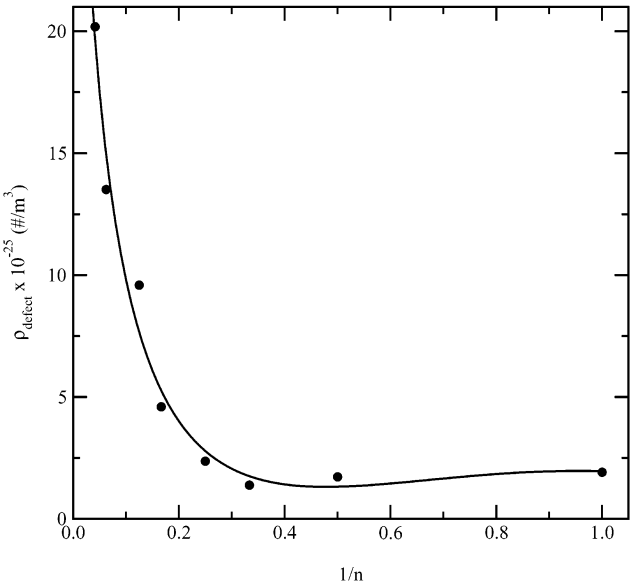

Figure 9. Defect density in the *n*-alkane inherent structures at their respective Sastry densities plotted as a function of inverse carbon number. The line is a guide to the eye.

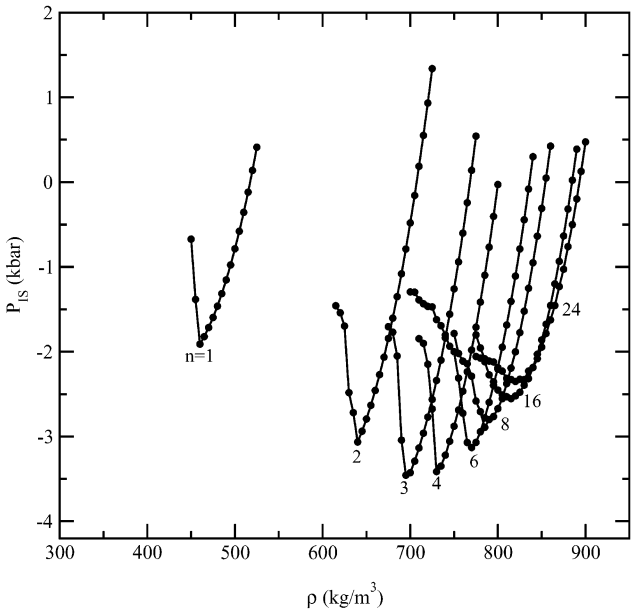

Figure 10. Inherent structure deformation curves for the *n*-alkanes of chain length $n = 1$, 2, 3, 4, 6, 8, 16, and 24.

molecules pack together directly affects their propensity to form voids and cavities which can lead to failure.

We have also determined the ultimate isotropic tensile strength by directly deforming *n*-alkane inherent structures for carbon numbers $n = 1$, 2, 3, 4, 6, 8, 16, and 24. Recall that the computational procedure consists of a series of isotropic expansion and energy minimization steps and, thus, closely resembles the experimental protocol one would use to measure isotropic tensile strength. These deformation curves are shown in Figure 10. In this case too, the ultimate isotropic tensile strength corresponds to the minimum in pressure, and the corresponding density is likewise analogous to the Sastry density. Statistical geometric analysis also shows that this density signals the sudden emergence of void space as the system is expanded isotropically. Although the deformation curves and the equations of state of the landscape have similar shapes, the deformation curves are noticeably sharper in the vicinity of the

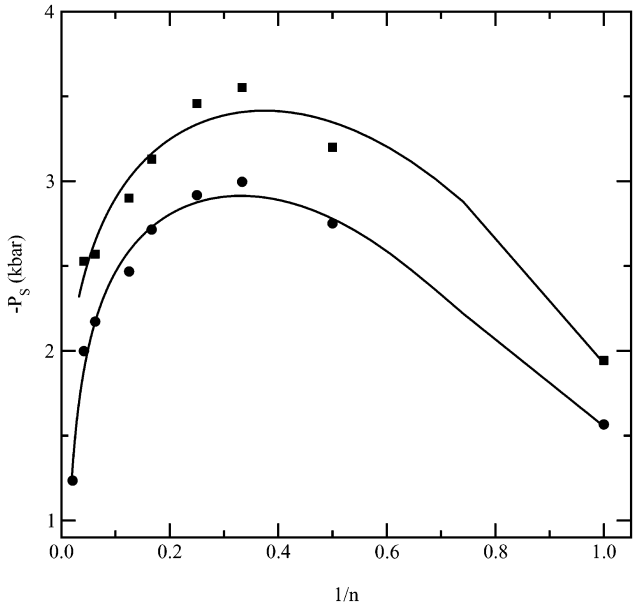

Figure 11. Comparison of the ultimate isotropic tensile strength determined by the landscape equation of state (circles) and direct inherent structure deformation (squares) versus inverse carbon number. Lines are guides to the eye.

pressure minimum, which is indicative of a brittle, catastrophic failure mode. Interestingly, the density at which fracture occurs, as determined by both constructions, is the same. We note that although each curve in Figure 10 represents an average over fifteen runs, the density at which each run fractured occurred over a range of values around the Sastry density. Moreover, this density range increased with chain length. In Figure 11, the tensile strengths calculated by the two methods are plotted simultaneously for comparison. The direct deformation process gives rise to a slightly greater tensile strength than that obtained by isochoric energy minimization (the equation of state of the landscape). Because the initial configuration of the deformation process is itself an inherent structure, the intuitive expectation is that the process is restricted at the outset to sample lower-lying energy basins. This is in contrast to the isochoric quench procedure, in which higher-energy minima are accessible during the high-temperature equilibration simulation that connects points along the equation of state of the energy landscape. To the extent that these lower-lying basins are closer to the ground state, and hence more crystal-like than the higher-energy ones, they represent "stronger" states.[48] This difference aside, the deformation curves and the landscape equation of state both predict the same nonmonotonic chain length dependence for the tensile strength, with a maximum at $n = 3$. For completeness, the defect densities at fracture for the two computational protocols are shown in Figure 12. Again, results generated by the two processes exhibit the same dependence on chain length. Also, in accord with the expectation that the defect density should correlate with material strength, the defect density at fracture by direct deformation is less than that observed in the landscape equation of state. As before, this correlation suggests that the nonmonotonic chain length dependence is related to molecular packing effects. In Appendix A, a simple theory that captures this nontrivial behavior and exposes the underlying physics is presented.

Because the extent of chain entanglement increases with chain length, the intuitive expectation is that ultimate tensile strength should increase with carbon number. We again point to the work of Klein and co-workers[30−33] who have investigated the effect

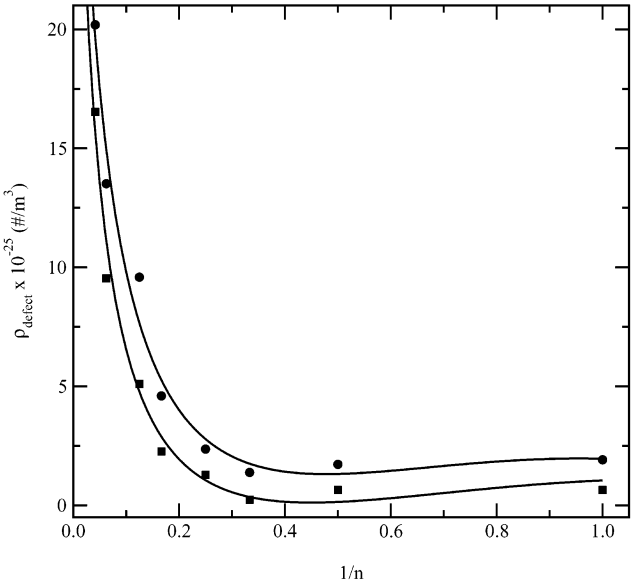

Figure 12. Comparison of the defect density at fracture for the equation of state of the energy landscape construction (circles) and the direct inherent structure deformation curve (squares). Lines are guides to the eye.

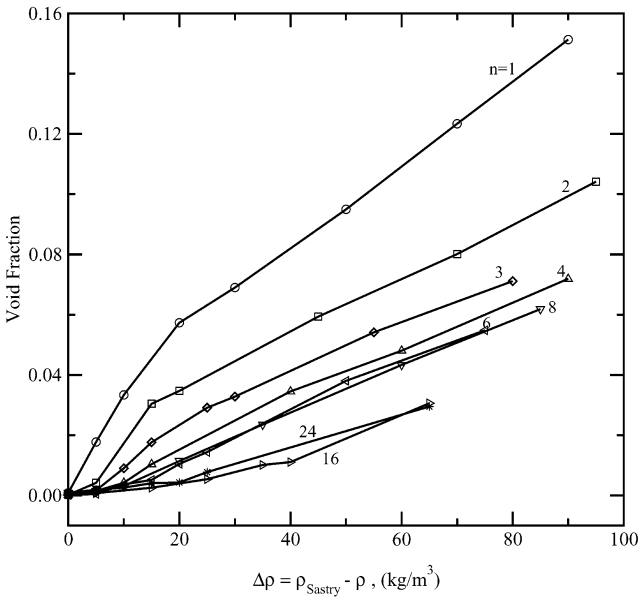

Figure 13. Evolution of void space beyond the Sastry density for the equation of state of the energy landscape of the *n*-alkanes.

of topological constraints, including chain entanglements and self-knots, on the rupture strength of the unsaturated carbon−carbon bond in *n*-alkane molecules ranging from $n = 9$ to $n = 35$. Their work suggests that chains of length greater than $n = 8$ should contain topological interchain entanglements, even though they might not exhibit rheological entanglement dynamics. Although the topological problem of identifying chain entanglements at the atomistic level remains unsolved,[37,80−86] visual inspection of the configurations for the longer chains, $n = 16$, 24, and 48, confirms that the molecules tend to adopt curled or folded conformations and tend to intertwine, indicating there is some degree of entanglement present. However, results from the landscape equations of state and the deformation curves show a counterintuitive trend, namely that the tensile strength decreases with chain length beyond $n = 3$. The disagreement between intuition and the results presented here stems from differences between the experimental and computational (this work) protocols used to measure ultimate strength. Experimentally, tensile strength tests are performed while deforming the specimen at a constant strain rate. The measurement is therefore a dynamical one. Thus, what is being measured is actually a time-dependent response to a perturbation. Because chain entanglements only affect the dynamic response of a system,[87] one should expect experimental measurements of tensile strength to increase with chain length if the time scale for chain relaxation is longer than that of the imposed strain rate. However, the computational methods employed here, namely construction of the landscape equations of state and the deformation curves, provide only static measures of material strength. It is important to emphasize that the equation of state of the energy landscape is a purely thermodynamic construction that corresponds to the zero-temperature isotherm of a liquid.[44] Ultimate tensile strength determined via this construct is based solely on thermodynamic stability. Although the inherent structure deformation curves were constructed using a protocol that more closely resembles an experimental isotropic tensile strength test, the procedure does not involve any dynamic component because after each deformation, the potential energy of the resulting structure is minimized, allowing the system to attain a mechanically stable condition. In other words, the inherent structure deformation curves correspond to the stress−strain curves one would generate in an experimental measurement using an infinitely slow strain rate, in the low-temperature limit. Because the computational procedures used in this work determine ultimate tensile strength within a purely thermodynamic framework, chain entanglements should not be expected to influence the predicted material strength. In fact, it might be more appropriate to refer to material strength measured within the inherent structure formalism as the material's *intrinsic* mechanical strength.

We now point out another interesting trend that can be seen in Figures 5 and 10. Looking at the equation of state of the energy landscape, Figure 5, it can be seen that the curves become smoother with increasing chain length, particularly on the low density side just after fracture. Although the deformation curves, Figure 10, are fairly sharp near the fracture point, the curvature clearly decreases with carbon number. This effect is a reflection of increasing material toughness, that is to say resistance to mechanical failure in the presence of a defect,[88] with chain length. In Figure 13, the evolution of void space beyond the Sastry density is shown for the isochoric energy minimization procedure. Notice the systematic decrease in slope with increasing chain length, indicating that systems composed of short chains are particularly susceptible to the creation of void space. The same qualitative trends are observed for the direct deformation process. Physically, the data point to the fact that systems composed of small molecules are unable to accommodate "internal" void space and simply come apart catastrophically. In contrast, as the density is lowered below the Sastry point, chain molecules partially unbind to create void space, but the voids thus created are not catastrophic. The constraints associated with chemical bonding serve as "stitching points" that hold the system together. Consequently, because the number of "stitching points" increases with chain length, it becomes increasingly difficult to create cavity space beyond that already present at the Sastry point.

It has been shown that the Sastry point for simple fluids practically coincides with the $T = 0$ limit of the superheated liquid spinodal and, hence, bears a simple relationship to the critical point.[42,44,48] In Figure 14, the ratios of the Sastry density to experimental critical density and the ultimate isotropic tensile

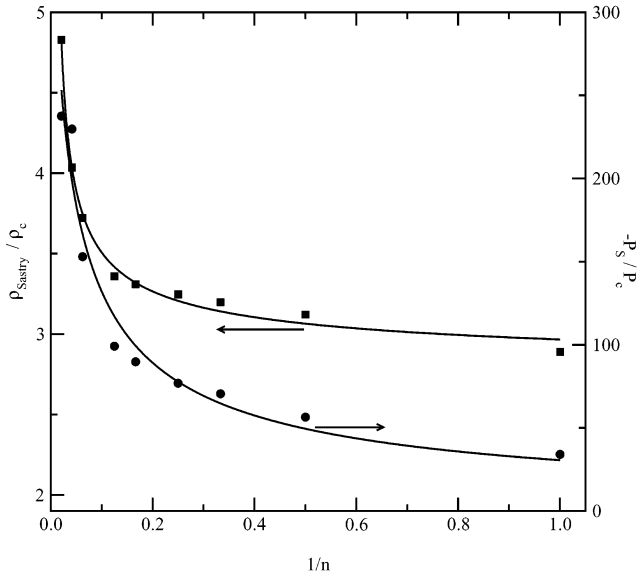

Figure 14. Ratios of the Sastry density to the experimental critical density (squares) and ultimate isotropic tensile strength to the experimental critical pressure (circles) as a function of inverse chain length for the *n*-alkanes. Lines are guides to the eye.

strength to experimental critical pressure are plotted as a function of chain length. The ratios for united atom methane ($\rho_S/\rho_C = 2.89$, $-P_S/P_C = 34$) are close to the corresponding values for the Lennard−Jones fluid ($\rho_S/\rho_C = 2.76$, $-P_S/P_C = 39.8$). Although the experimental critical density and pressure of the *n*-alkanes both depend nonmonotonically on chain length, it is interesting to see that both Sastry-to-critical point ratios increase monotonically with carbon number and appear to diverge in the infinitely long chain limit. Vega and co-workers[89,90] have shown that the critical density and pressure of the *n*-alkanes scale as $n^{-3/2}$ in the long-chain limit. Because the Sastry density reaches a plateau value, the ratio ρ_S/ρ_C should indeed diverge in the limit of large *n*. However, based on our tensile strength calculations, it is not clear a priori how the ratio $-P_S/P_C$ should behave in the infinitely long chain limit. We can deduce that the scaling exponent for $-P_S$ as a function of *n* is less than 3/2.

The chain length dependence of the maximum in ultimate isotropic tensile strength, $-P_S$, within the family of *n*-alkane glasses is a surprising result and has yet to be confirmed experimentally. Microscopic theories designed to capture the liquid−vapor phase behavior of simple molecular fluids, such as that of Sanchez−Lacombe,[91] do not predict complex chain length dependence of the pressure in the $T = 0$ limit of the superheated liquid spinodal and thus the underlying physics is not at all obvious. To elucidate the underlying physics, it is useful to examine the relationship between tensile strength $-P_S$ and the cohesive energy density δ^2 which is defined thermodynamically to be

$$\delta^2 \equiv \frac{\Delta U^{\text{vaporization}}}{V^{\text{L}}} \tag{10}$$

where $\Delta U^{\text{vaporization}}$ is the internal energy change of vaporization for a volume of liquid V^L. Physically, δ^2 is just a measure of the strength of the intermolecular interactions in the liquid phase. If the vapor is considered ideal, then the cohesive energy density reduces to

$$\delta^2 = \frac{-E^{\text{L}}_{\text{intermolecular}}}{V^{\text{L}}} \tag{11}$$

where $E^{\text{L}}_{\text{intermolecular}}$ is the total intermolecular interaction energy in the liquid. For small molecules and within small density ranges, the cohesive energy density is proportional to the partial derivative of the total internal energy of the liquid with respect to volume at constant temperature[92]

$$\delta^2 = a\left(\frac{\partial U}{\partial V}\right)_T \tag{12}$$

where the proportionality constant *a* is close to unity. In fact, for the van der Waals fluid it is exactly unity. Using the differential form of the fundamental equation $U(S,V)$, where *S* is the entropy, and a Maxwell relation,[93] it is straightforward to show that

$$\left(\frac{\partial U}{\partial V}\right)_T = T\left(\frac{\alpha_P}{\kappa_T}\right) - P \tag{13}$$

where α_P is the thermal expansion coefficient and κ_T is the isothermal compressibility. Exploiting the fact that the equation of state of the energy landscape is the $T = 0$ isotherm for a liquid, the ultimate isotropic tensile strength becomes

$$-P_S = \left(\frac{\partial U}{\partial V}\right)_T \tag{14}$$

A subtle point to note in moving from eq 13 to 14 is that the Sastry point is a limit of mechanical stability, and thus, both the thermal expansion coefficient and the isothermal compressibility diverge there. It is therefore unclear how the ratio of these two quantities behaves in the limit of the $T = 0$ superheated liquid spinodal. However, we can deduce how the ratio α_P/κ_T behaves in this limit by examining its behavior for two model fluids with intermolecular potentials that bracket the range of reasonable repulsive interactions in real systems. To this end, the van der Waals fluid and the soft sphere fluid consisting of an inverse ninth-power repulsion with a mean-field attraction were examined. By definition, the ratio α_P/κ_T is just the partial derivative of pressure with respect to temperature at constant density $(\partial P/\partial T)_\rho$. Because the equation of state of a fluid can generally be expressed in terms of pressure as a function of density and temperature, $P(\rho,T)$, the total differential of pressure is

$$dP = \left(\frac{\partial P}{\partial T}\right)_\rho dT + \left(\frac{\partial P}{\partial \rho}\right)_T d\rho \tag{15}$$

Along the liquid spinodal where $(\partial P/\partial \rho)_T = 0$, eq 15 reduces to

$$\left(\frac{dP}{dT}\right)_{\text{sp}} = \left(\frac{\partial P}{\partial T}\right)_\rho \tag{16}$$

which states that the pressure−temperature projection of the liquid spinodal curve is an envelope of isochores.[7] Using the chain rule, eq 16 can be rewritten as

$$\left(\frac{\partial P}{\partial T}\right)_\rho = \left(\frac{dP}{d\rho}\right)_{\text{sp}}\left(\frac{d\rho}{dT}\right)_{\text{sp}} \tag{17}$$

For the van der Waals equation of state, one can show that the ratio α_P/κ_T diverges at the Sastry density in the limit of $T = 0$. However, it does so as $T^{-1/2}$, and so the term $T(\alpha_P/\kappa_T)$ in eq 13 vanishes as $T \rightarrow 0$. For the soft sphere fluid, we have verified numerically that α_P/κ_T does not diverge but approaches a finite value in this limit. Therefore, we assume the general validity

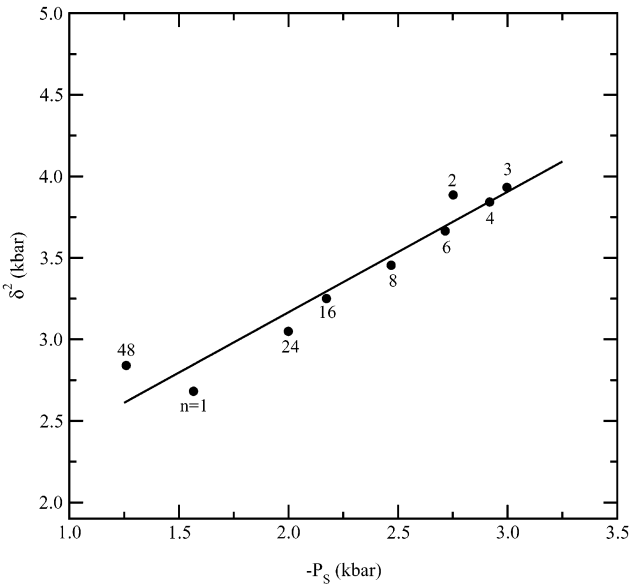

Figure 15. Correlation between ultimate isotropic tensile strength determined by the isochoric quench process and cohesive energy density for the *n*-alkanes studied in this work.

of this conclusion, and assume that the first term on the right-hand side of eq 13 vanishes at the Sastry density as $T \rightarrow 0$. It then follows that

$$P_S = \frac{1}{a}\frac{E^L_{\text{intermolecular}}}{V^L} \tag{18}$$

To test this result, we plot the tensile strength against the corresponding cohesive energy density in Figure 15. The linear correlation is quite good, suggesting that in order to explain the tensile strength maximum at $n = 3$, one simply needs to develop a theory for the chain length dependence of the cohesive energy density.

In Appendix A, a simple theory capable of reproducing the maximum in cohesive energy, and therefore tensile strength, is presented. Here, we briefly summarize its key points. Notice in eq 18 that the ultimate isotropic tensile strength has been decomposed into energetic and geometric contributions. Each is treated separately in the theory. The energetic contribution to the cohesive energy density is calculated by making an analogy to the conceptual framework of lattice models where it is assumed each lattice site is occupied by a chain segment. Invoking a simple mean field approximation, the average intermolecular interaction energy per molecule can be calculated while accounting for different characteristic interaction energies for the methyl and methylene groups. The geometric contribution to the cohesive energy density, or the total volume of the system, is approximated as a simple summation over all molecular volumes, accounting for the fact that adjacent pairs of united atoms within the same molecule overlap (i.e., they are interpenetrating spheres by virtue of chemical bonding). Within this simple framework, the theory is not only able to reproduce a maximum in cohesive energy density at $n = 3$, but also predicts that the cohesive energy density, and therefore tensile strength, decreases with chain length beyond $n = 3$ and approaches a finite asymptotic value as $n \rightarrow \infty$. Furthermore, when extended to calculate the Sastry density, the theory predicts the same qualitative behavior as observed in the simulations, namely that ρ_S initially increases with carbon number and then reaches a plateau value.

As shown in Appendix A, these simple arguments allow the cohesive energy density to be written in the following general form

$$\delta^2(n) = \xi(n)\omega(n) \tag{19}$$

where $\xi(n)$ is defined as the negative of the average intermolecular interaction energy per united atom within a chain, and $\omega(n)$ is the intramolecular united atom, or carbon, density. The maximum in tensile strength is just a reflection of the competition between these energetic and intramolecular packing contributions. The average intermolecular interaction energy per carbon $\xi(n)$ decreases with chain length simply because the characteristic interaction energy of a methyl group is less than that of a methylene group, which is consistent with other force fields used to simulate hydrocarbons. This tends to decrease δ^2 with increasing carbon number. On the other hand, the average intramolecular carbon density behaves much like the Sastry density and increases with chain length mainly due to intramolecular packing effects, that is to say how the united atoms fit together within a chain, and this tends to cause δ^2 to increase with carbon number. The consequence of this competition naturally gives rise to a maximum. In the situation where the characteristic energies of the methyl and methylene groups are equal, the theory predicts that δ^2 increases monotonically with carbon number and should track the behavior of the Sastry density. In fact, we have located the Sastry point for the *n*-alkane simulation model with this energetic modification for $n = 1$, 2, 3, 4, 8, and 16. We find that the Sastry density is largely insensitive to the energetics of the model. More importantly, as predicted by the theory, the ultimate isotropic tensile strength in this case initially increases with chain length and then flattens out, much like the Sastry density.

V. Conclusions

A systematic study of the ultimate isotropic tensile strength of *n*-alkane glasses up to $n = 48$ has been performed. We have shown that the equation of state of the energy landscape and the inherent structure deformation curve provide two independent measures of the isotropic tensile strength for these glasses. In particular, it is the pressure minimum in both curves that corresponds to the maximum isotropic tension that a system can sustain prior to fracture. Although both methods predict the same density at which fracture occurs, the deformation curve systematically predicts a higher tensile strength than the landscape equation of state simply because the process is biased to sample basins of lower energy. This difference aside, both constructions exhibit similar trends with respect to the Sastry density and tensile strength dependence on chain length. The Sastry density initially increases with carbon number and then reaches a plateau value at some intermediate carbon number. More interesting, however, is the nonmonotonic chain length dependence of the ultimate isotropic tensile strength with a maximum at $n = 3$, which is reminiscent of the maximum in critical pressure at $n = 2$ for this homologous series. By relating the cohesive energy to pressure in the zero-temperature limit, it can be shown by means of a simple theory that the observed chain length dependence of the Sastry point is driven by a competition between intermolecular energetic and intramolecular packing effects. Although the results seem to contradict intuitive expectations regarding the connection between mechanical strength and molecular structure, in particular, the notion that strength should increase with chain length, the crucial distinction between the actual experimental protocol and computational

methods used here is the following. Experimental measurements inevitably are determined while the sample is deformed at an externally imposed strain rate, and the measured strength is therefore a reflection of the dynamic response of the system to a perturbation. It should therefore be expected that features such as chain entanglements and even cross-links increase the experimentally observed tensile strength. In this work, mechanical strength has been determined within a purely static framework and ultimate strength corresponds to a limit of mechanical stability. Because the computational protocols used in this work correspond to an experimental measurement using an infinitely slow strain rate, points of chain entanglements are always allowed to relax, and thus do not influence the intrinsic tensile strength.

From an interesting theoretical perspective, we have shown that the relationship between the Sastry point and the critical point is more complex for molecular than for monatomic fluids. Both ratios, ρ_S/ρ_C and $-P_S/P_C$, diverge in the infinitely long chain limit. Combined with theoretical work by Vega and coworkers[89,90] showing that the critical density and critical pressure for the *n*-alkanes scale as $n^{-3/2}$, this behavior should be expected in light of the theory for tensile strength summarized in Section IV and presented in Appendix A which predicts an asymptotic approach to a limiting value as $n \rightarrow \infty$.

A number of interesting issues are raised by this work and deserve further investigation. Experimentally, the ultimate strength of a material usually refers to its mechanical response under uniaxial loading. Shear strength is also an important mechanical property in engineering applications. These particular properties can be determined using the inherent structure formalism, and it would be interesting to see if they exhibit complex chain length dependence. We have also pointed out that the equations of state of the energy landscape and the inherent structure deformation curves become smoother with carbon number, particularly just after the point of fracture. This smoothing effect is believed to be associated with "stitching points" provided by longer chain molecules by virtue of chemical bonds which serve to hold the system together. The implication of this subtle trend is that amorphous solids composed of longer chains are mechanically tougher, that is to say less susceptible to mechanical failure when a void defect is present, than shorter, smaller molecules. Experimental studies of the chain-length dependence of toughness are necessary to confirm or disprove this prediction.

Appendix A: Mean-Field Theory for Cohesive Density

In this appendix, we present a simple mean-field theory capable of capturing the qualitative behavior of the cohesive energy density, and therefore tensile strength, as a function of chain length. The starting point for this theory is eq 18 which decomposes the cohesive energy density into purely energetic and geometric contributions, each of which is treated independently in what follows.

The total intermolecular interaction energy is calculated using a simple mean-field approximation. To facilitate such a calculation, we make an analogy to the conceptual framework of lattice models, where we crudely assume that each chain segment occupies a lattice site. All sites are assumed to be occupied because the system of interest is at its Sastry density, where the only voids are interstitial. Surrounding each site are *z* near-neighbors. In this work, we take the coordination number to be an adjustable parameter.[94] For a chain of length $n > 2$, there are two CH_3 groups and (n-2) CH_2 groups. Intermolecular methyl−methyl interactions have a characteristic energy ϵ_{11}, and methylene-methylene interactions are characterized by an energy ϵ_{22}. A geometric mean is used to define interactions between different united atoms

$$\epsilon_{12} = \sqrt{\epsilon_{11}\epsilon_{22}} \tag{A1}$$

In a mean-field sense, the probability, $p_1(n)$, that a near-neighbor lattice site is occupied by a CH_3 group of another molecule is

$$p_1(n) = \frac{2}{n} \tag{A2}$$

Accordingly, the probability, $p_2(n)$, that a near-neighbor site is occupied by a CH_2 group of another molecule is

$$p_2(n) = \frac{n-2}{n} \tag{A3}$$

The average intermolecular interaction energy per molecule, $\phi(n)$, due to near-neighbor interactions is therefore

$$-\frac{\phi(n)}{\epsilon_{11}} = \frac{(n-2)(z-2)}{2}\left[p_1(n)\left(\frac{\epsilon_{22}}{\epsilon_{11}}\right)^{1/2} + p_2(n)\left(\frac{\epsilon_{22}}{\epsilon_{11}}\right)\right] + \frac{(z-1)}{2}\left[p_1(n) + p_2(n)\left(\frac{\epsilon_{22}}{\epsilon_{11}}\right)^{1/2}\right] \tag{A4}$$

Note that a factor of has been included to account for double counting. Analogous expressions for united atom methane and ethane can be easily derived. The total intermolecular interaction energy for the system is

$$E^{L}_{\text{intermolecular}} = N_{\text{mol}}\phi(n) \tag{A5}$$

where N_{mol} is the number of molecules in the system.

Because the Sastry point is the lowest density at which a homogeneous glass can exist, that is to say it corresponds to the onset of void formation, the total volume of the system is approximated as a simple summation over all molecular volumes. Implicit in this approximation is the assumption that although intermolecular overlaps do exist, the overlap volume occupies only a small fraction of the total system volume which is largely composed of the volume of the molecules themselves. The average molecular volume can be written in the following general form

$$\upsilon(n) = \upsilon_{\text{tangent}}(n) - \upsilon_{\text{overlap}}(n) \tag{A6}$$

where $\upsilon_{\text{tangent}}(n)$ is the average molecular volume calculated by assuming the united atoms are tangent spheres and $\upsilon_{\text{overlap}}(n)$ is the average total overlap volume between adjacent sites in a chain and is important in this particular case because of chemical bonding. For simplicity, only overlaps between adjacent pairs of united atoms sites are considered. Given the schematic setup in Figure A1, the overlap volume υ_o between two interpenetrating spheres of radii r_1 and r_2 whose centers are separated by a distance d is

$$\upsilon_o = \pi\{\int_0^{y_c} dy[r_2^2 - (y - r_2)^2] + \int_{y_c}^{y_t} dy[r_1^2 - (y - [r_2 - d])^2]\} \tag{A7}$$

where

$$y_c = \frac{1}{2}\left[\frac{(r_1 + r_2)(r_1 - r_2)}{d} + (2r_2 - d)\right] \tag{A8}$$

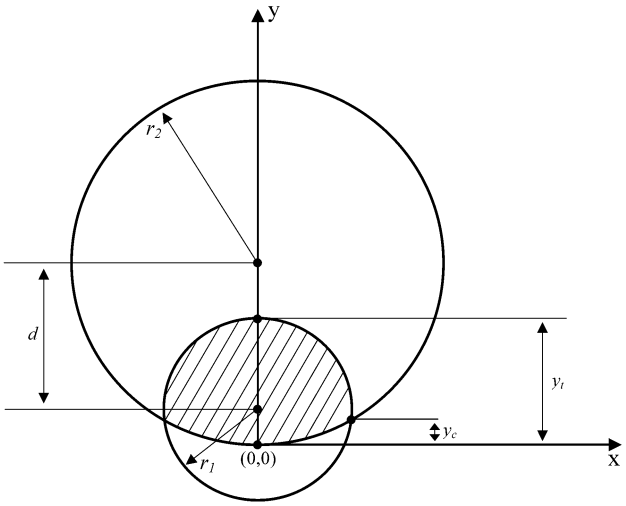

Figure A1. Two-dimensional schematic setup for calculating the overlap volume between two interpenetrating spheres of radii r_1 and r_2, with centers separated a distance d from each other. The shaded region corresponds to the overlap volume in three dimensions.

and

$$y_t = r_1 + (r_2 - d) \tag{A9}$$

The total overlap volume within a molecule is therefore just a summation over all adjacent united atom pairs. In the present context, the natural length scale is assumed to be the radius of the united atom's exclusion sphere, which is of the order of the Lennard−Jones diameter σ. Such a choice is consistent with the statistical geometric analysis already performed that demonstrates the emergence of void space at the Sastry density. The radius of a CH_3 group is denoted by σ_1 and that of a CH_2 group by σ_2. It naturally follows that the system volume is

$$V^{\mathrm{L}} = N_{\mathrm{mol}} v(n) \tag{A10}$$

Combining eqs 18, A5, and A10, a closed-form expression for the cohesive energy density as a function carbon number can be obtained

$$\delta^2(n) = \frac{-\phi(n)}{v(n)} \tag{A11}$$

where the proportionality constant a in eq 18 is taken to be of order unity. Notice that the cohesive energy density is now expressed as the ratio of single-molecule quantities. The relative sizes and characteristic energies of the united atom types in the theory are set to be consistent with the simulation model. The only adjustable parameters in the theory are the coordination number z and equilibrium bond lengths, which are chosen to be species-specific. To fit the cohesive energy data, the optimum values for the bond lengths between CH_3-CH_3, CH_3-CH_2, and CH_2-CH_2 groups were found to be 0.140, 0.590, and 0.265 σ_1, respectively, for a "coordination number" $z = 51$. We note that the value of z does not affect the qualitative behavior as a function of chain length and only scales up or down the value of the cohesive energy density. This is consistent with previous studies that have shown using the coordination number as an adjustable parameter does not affect qualitative trends but only serves to improve agreement between theory and experiment.[94] With these parameters, eq A11 exhibits a maximum at $n = 3$. Beyond $n = 3$, the theory predicts that the cohesive energy density actually decreases monotonically with carbon number and approaches a finite value in the infinitely long chain limit. This behavior is consistent with observed trends for solubility parameter calculations in polymeric systems.[95] Because the system volume at the Sastry point is calculated explicitly, the theory can also be used to determine the Sastry density. It is straightforward to show that the Sastry density predicted by this theory initially increases with chain length and then reaches a plateau value in the long-chain limit.

It has already been pointed out in Section IV how packing effects relate to the behavior of the Sastry density as a function of carbon number. However, more intriguing is the ultimate tensile strength, and therefore cohesive energy density, maximum at $n = 3$. The underlying physics that give rise to this maximum can be elucidated by multiplying and dividing eq A11 by n

$$\delta^2(n) = \xi(n)\omega(n) \tag{A12}$$

where $\xi(n) = -\phi(n)/n$ and $\omega(n) = n/v(n)$. Physically, $\xi(n)$ is just the intermolecular energy per united atom within a chain, and $\omega(n)$ is just the intramolecular united atom, or carbon, density. As pointed out in Section IV, the maximum in tensile strength is a simple consequence of the competition between these energetic and intramolecular packing contributions. Because $\epsilon_{22} < \epsilon_{11}$, $\xi(n)$ decreases with n. On the other hand, the average intramolecular carbon density $\omega(n)$ behaves much like the Sastry density due to intramolecular packing effects and increases with chain length. Therefore, the product of these two contributions gives rise to a maximum. Although the present theory is by no means rigorous, it is a simple, physically based theory that simultaneously captures the complex chain length dependence of the tensile strength and Sastry density observed in our simulations.

Acknowledgment. P.G.D. gratefully acknowledges the financial support of the U. S. Department of Energy, Division of Chemical Sciences, Geosciences, and Biosciences, Office of Basic Energy Sciences (Grant No. DE-FG02-87ER13714).

References and Notes

(1) Kirk, R. E.; Othmer, D. F.; Kroschwitz, J. I.; Howe-Grant, M. *Encyclopedia of Chemical Technology*, 4th ed.; Wiley: New York, 1992.
(2) Franks, F. *Biotechnology* **1994**, *12*, 253.
(3) Chaudhari, P.; Turnbull, D. *Science* **1978**, *199*, 11.
(4) Greer, A. L. *Science* **1995**, *267*, 1947.
(5) Zarzycki, J. *Glasses and the Vitreous State*; Cambridge University Press: Cambridge, New York, 1991.
(6) Angell, C. A. *Science* **1995**, *267*, 1924.
(7) Debenedetti, P. G. *Metastable Liquids: Concepts and Principles*; Princeton University Press: Princeton, NJ, 1996.
(8) Courtney, T. H. *Mechanical Behavior of Materials*; McGraw-Hill: New York, 1990.
(9) Hertzberg, R. W. *Deformation and Fracture Mechanics of Engineering Materials*, 4th ed.; John Wiley & Sons: New York, 1996.
(10) Scherer, G. W. *Relaxation in Glass and Composites*; Wiley: New York, 1986.
(11) Hill, R.; Milstein, F. *Phys. Rev. B* **1977**, *15*, 3087.
(12) Nielsen, O. H.; Martin, R. M. *Phys. Rev. B* **1985**, *32*, 3780.
(13) Roundy, D.; Krenn, C. R.; Cohen, M. L.; Morris, J. W. *Phys. Rev. Lett.* **1999**, *82*, 2713.
(14) Telling, R. H.; Pickard, C. J.; Payne, M. C.; Field, J. E. *Phys. Rev. Lett.* **2000**, *84*, 5160.
(15) Chacham, H.; Kleinman, L. *Phys. Rev. Lett.* **2000**, *85*, 4904.
(16) da Silva, E. Z.; da Silva, A. J. R.; Fazzio, A. *Phys. Rev. Lett.* **2001**, *8725*, 6102.
(17) Roundy, D.; Cohen, M. L. *Phys. Rev. B* **2001**, *6421*, 2103.
(18) Selinger, R. L. B.; Wang, Z. G.; Gelbart, W. M. *J. Chem. Phys.* **1991**, *95*, 9128.
(19) Wang, Z. G.; Landman, U.; Selinger, R. L. B.; Gelbart, W. M. *Phys. Rev. B* **1991**, *44*, 378.
(20) Selinger, R. L. B.; Wang, Z. G.; Gelbart, W. M.; Benshaul, A. *Phys. Rev. A* **1991**, *43*, 4396.

(21) Lynden-Bell, R. M. *J. Phys. Condens. Matter* **1995**, *7*, 4603.
(22) Lynden-Bell, R. M. *Science* **1994**, *263*, 1704.
(23) Romano, A.; Li, J.; Yip, S. *Physica A* **2002**, *304*, 11.
(24) Selinger, R. L. B.; Lynden-Bell, R. M.; Gelbart, W. M. *J. Chem. Phys.* **1993**, *98*, 9808.
(25) Abraham, F. F.; Walkup, R.; Gao, H.; Duchaineau, M.; De La Rubia, T. D.; Seager, M. *P. Natl. Acad. Sci. U.S.A.* **2002**, *99*, 5777.
(26) Abraham, F. F.; Walkup, R.; Gao, H.; Duchaineau, M.; De La Rubia, T. D.; Seager, M. *P. Natl. Acad. Sci. U.S.A.* **2002**, *99*, 5783.
(27) Theodorou, D. N.; Suter, U. W. *Macromolecules* **1985**, *18*, 1467.
(28) Theodorou, D. N.; Suter, U. W. *Macromolecules* **1986**, *19*, 379.
(29) Theodorou, D. N.; Suter, U. W. *Macromolecules* **1986**, *19*, 139.
(30) Saitta, A. M.; Soper, P. D.; Wasserman, E.; Klein, M. L. *Nature* **1999**, *399*, 46.
(31) Saitta, A. M.; Klein, M. L. *J. Chem. Phys.* **1999**, *111*, 9434.
(32) Saitta, A. M.; Klein, M. L. *J. Phys. Chem. B* **2000**, *104*, 2197.
(33) Saitta, A. M.; Klein, M. L. *J. Phys. Chem. B* **2001**, *105*, 6495.
(34) Termonia, Y.; Meakin, P.; Smith, P. *Macromolecules* **1985**, *18*, 2246.
(35) Termonia, Y.; Smith, P. *Macromolecules* **1987**, *20*, 835.
(36) Terzis, A. F.; Theodorou, D. N.; Stroeks, A. *Macromolecules* **2000**, *33*, 1385.
(37) Terzis, A. F.; Theodorou, D. N.; Stroeks, A. *Macromolecules* **2000**, *33*, 1397.
(38) Terzis, A. F.; Theodorou, D. N.; Stroeks, A. *Macromolecules* **2002**, *35*, 508.
(39) Stillinger, F. H.; Weber, T. A. *Phys. Rev. A* **1982**, *25*, 978.
(40) Stillinger, F. H.; Weber, T. A. *Science* **1984**, *225*, 983.
(41) Debenedetti, P. G.; Stillinger, F. H. *Nature* **2001**, *410*, 259.
(42) Debenedetti, P. G.; Truskett, T. M.; Lewis, C. P.; Stillinger, F. H. *Adv. Chem. Eng.* **2001**, *28*, 21.
(43) Sastry, S.; Debenedetti, P. G.; Stillinger, F. H. *Phys. Rev. E* **1997**, *56*, 5533.
(44) Debenedetti, P. G.; Stillinger, F. H.; Truskett, T. M.; Roberts, C. J. *J. Phys. Chem. B* **1999**, *103*, 7390.
(45) La Nave, E.; Mossa, S.; Sciortino, F. *Phys. Rev. Lett.* **2002**, *88*, 225 701.
(46) La Violette, R. A.; Budzien, J. L.; Stillinger, F. H. *J. Chem. Phys.* **2000**, *112*, 8072.
(47) Roberts, C. J.; Debenedetti, P. G.; Stillinger, F. H. *J. Phys. Chem. B* **1999**, *103*, 10 258.
(48) Utz, M.; Debenedetti, P. G.; Stillinger, F. H. *J. Chem. Phys.* **2001**, *114*, 10 049.
(49) Earnshaw, J. C.; Hughes, C. J. *Phys. Rev. A* **1992**, *46*, R4494.
(50) Ocko, B. M.; Wu, X. Z.; Sirota, E. B.; Sinha, S. K.; Gang, O.; Deutsch, M. *Phys. Rev. E* **1997**, *55*, 3164.
(51) Maeda, N.; Yaminsky, V. V. *Phys. Rev. Lett.* **2000**, *84*, 698.
(52) Sloutskin, E.; Sirota, E. B.; Kraack, H.; Ocko, B. M.; Deutsch, M. *Phys. Rev. E* **2001**, *6403*, 1708.
(53) Gang, H.; Patel, J.; Wu, X. Z.; Deutsch, M.; Gang, O.; Ocko, B. M.; Sirota, E. B. *Europhys. Lett.* **1998**, *43*, 314.
(54) Farkas, A. *Physical Chemistry of the Hydrocarbons*; Academic Press: New York, 1950.
(55) *CRC Handbook of Chemistry and Physics*, 70 ed.; CRC Press: Cleveland, Ohio, 1989; pp v.
(56) Lemmon, E. W.; Goodwin, A. R. H. *J. Phys. Chem. Ref Data* **2000**, *29*, 1.
(57) Pamies, J. C.; Vega, L. F. *Ind. Eng. Chem. Res.* **2001**, *40*, 2532.
(58) Vega, C.; MacDowell, L. G. *Mol. Phys.* **1996**, *88*, 1575.
(59) Stillinger, F. H.; Weber, T. A. *Phys. Rev. A* **1983**, *28*, 2408.
(60) Malandro, D. L.; Lacks, D. J. *J. Chem. Phys.* **1997**, *107*, 5804.
(61) La Nave, E.; Scala, A.; Starr, F. W.; Sciortino, F.; Stanley, H. E. *Phys. Rev. Lett.* **2000**, *84*, 4605.
(62) Scala, A.; Starr, F. W.; La Nave, E.; Sciortino, F.; Stanley, H. E. *Nature* **2000**, *406*, 166.
(63) Kieffer, J.; Angell, C. A. *J. Non-Cryst. Solids* **1988**, *106*, 336.
(64) Lacks, D. J. *Phys. Rev. Lett.* **1998**, *80*, 5385.
(65) Malandro, D. L.; Lacks, D. J. *J. Chem. Phys.* **1999**, *110*, 4593.
(66) Gagnon, G.; Patton, J.; Lacks, D. J. *Phys. Rev. E* **2001**, *6405*, 1508.
(67) Nath, S. K.; Escobedo, F. A.; de Pablo, J. J. *J. Chem. Phys.* **1998**, *108*, 9905.
(68) Vanderploeg, P.; Berendsen, H. J. C. *J. Chem. Phys.* **1982**, *76*, 3271.
(69) Errington, J. R.; Panagiotopoulos, A. Z. *J. Phys. Chem. B* **1999**, *103*, 6314.
(70) Jorgensen, W. L.; Madura, J. D.; Swenson, C. J. *J. Am. Chem. Soc.* **1984**, *106*, 6638.
(71) Errington, J. R.; Panagiotopoulos, A. Z. *J. Chem. Phys.* **1998**, *109*, 1093.
(72) Martin, M. G.; Siepmann, J. I. *J. Phys. Chem. B* **1998**, *102*, 2569.
(73) Siepmann, J. I.; Frenkel, D. *Mol. Phys.* **1992**, *75*, 59.
(74) Frenkel, D.; Smit, B. *Understanding Molecular Simulation: From Algorithms to Applications*, 2nd ed.; Academic Press: San Diego, 2002.
(75) Tuckerman, M. E.; Martyna, G. J. *J. Phys. Chem. B* **2000**, *104*, 159.
(76) Martyna, G. J.; Tuckerman, M. E.; Tobias, D. J.; Klein, M. L. *Mol. Phys.* **1996**, *87*, 1117.
(77) Press, W. H. *Numerical Recipes in Fortran: The Art of Scientific Computing*, 2nd ed.; Cambridge University Press: Cambridge, New York, 1992.
(78) Sastry, S.; Corti, D. S.; Debenedetti, P. G.; Stillinger, F. H. *Phys. Rev. E* **1997**, *56*, 5524.
(79) Popli, R.; Mandelkern, L. *J. Polym. Sci. Pol. Phys.* **1987**, *25*, 441.
(80) Edwards, S. F. *P. Roy. Soc. Lond. a Mat.* **1983**, *385*, 267.
(81) Kavassalis, T. A.; Noolandi, J. *Phys. Rev. Lett.* **1987**, *59*, 2674.
(82) Iwata, K.; Edwards, S. F. *J. Chem. Phys.* **1989**, *90*, 4567.
(83) Kremer, K.; Grest, G. S. *J. Chem. Phys.* **1990**, *92*, 5057.
(84) Wool, R. P. *Macromolecules* **1993**, *26*, 1564.
(85) Shaffer, J. S. *J. Chem. Phys.* **1994**, *101*, 4205.
(86) Padding, J. T.; Briels, W. J. *J. Chem. Phys.* **2001**, *115*, 2846.
(87) Doi, M.; Edwards, S. F. *The Theory of Polymer Dynamics*; Clarendon Press: Oxford University Press: Oxford Oxfordshire,New York, 1986.
(88) Callister, W. D. *Materials Science and Engineering: An Introduction*, 3rd ed.; Wiley: New York, 1994.
(89) MacDowell, L. G.; Muller, M.; Vega, C.; Binder, K. *J. Chem. Phys.* **2000**, *113*, 419.
(90) Vega, C.; McBride, C.; MacDowell, L. G. *Phys. Chem. Chem. Phys.* **2002**, *4*, 853.
(91) Sanchez, I. C.; Lacombe, R. H. *J. Phys. Chem.-Us* **1976**, *80*, 2352.
(92) Hildebrand, J. H.; Scott, R. L. *The Solubility of Nonelectrolytes*, 3rd ed.; Reinhold: New York, 1950.
(93) Tester, J. W.; Modell, M. *Thermodynamics and Its Applications*, 3rd ed.; Prentice Hall PTR: Upper Saddle River, NJ, 1997.
(94) Kumar, S. K.; Suter, U. W.; Reid, R. C. *Ind. Eng. Chem. Res.* **1987**, *26*, 2532.
(95) Spyriouni, T.; Vergelati, C. *Macromolecules* **2001**, *34*, 5306.